Lagrangian Methods in Experimental Fluid Mechanics

M. Bourgoin[1], J.-F. Pinton[2], R. Volk[2]

Abstract. High resolution methods have had a large impact in fluid mechanics over the past ten years. In this review, we concentrate on the Lagrangian approaches. Several strategies using optics, acoustics and even remote sensing are developed, giving access to the time solved dynamics of tracers and objects passively advected by fluid motions. Applications range from the understanding of phenomena such as dispersion of particles to the mixing of scalar fields and reactive processes.

1. Introduction

In the last decades, modeling and numerical simulations in fluid mechanics, have known an impressive increase of performances allowing important advances in computational fluid dynamics (CFD). At the same time, this progress has naturally generated an increasing demand of accuracy and reliability of existing models. Among these new requirements, an important challenge is the ability to describe more accurately systems with higher complexity, in terms for instance of non-homogeneities, anisotropy and turbulence effects, which are of particular importance in the context of geophysical flows. Improving our modeling capabilities therefore still relies on experimental investigations, which ought to be ever more accurate in order to identify and characterize ever subtler physical mechanisms.

This stimulates a permanent effort in the fluid mechanics experimental community, to constantly develop measurements with increasing accuracy and resolution. A particular challenge concerns the improvement of the multi-scale description of flows and of energy cascade mechanisms. Geophysical flows are indeed characterized by a high turbulence intensity which results in a important hierarchy of relevant scales, with structures ranging from kilometers down to millimeters. In turbulent flows, the range of relevant scales (called the *inertial range*) between the energy injection scale L and the dissipative scale (also called Kolmogorov scale) η is directly related to the Reynolds number, Re of the flow: $L/\eta \propto Re^{3/4}$ [*Tennekes and Lumley*, 1992]. Reynolds numbers of the order 10^6 are usual in geophysical flows, implying that at least 4 decades of spatial dynamics are typically involved. Similarly, concerning the temporal dynamics, the ratio between the eddy turnover time T_L at injection scale and at dissipation scales τ_η goes as $T_L/\tau_\eta \propto Re^{1/2}$, implying three decades of temporal dynamics. These dynamical ranges can be even further extended toward the largest scales due to inverse cascade mechanisms, which may become important for instance in the atmosphere, at scales where it dynamics exhibits 2D-properties, where flow structures can extend over hundreds of kilometers. When it comes to investigate related physics in laboratory experiments, with a typical dimension of the order of 1 m and typical correlation time scale of the order of 1 s, the investigation of a comparable hierarchy of scales pushes the smallest involved structures down to tens to hundreds of microns (or even smaller) in space with a typical time-scale of fractions of milliseconds. Recent technological advances in terms of high speed digital imaging in the last decade, with the capacity to record images with millions of pixels of spatial resolution at several thousands of frames per second has definitely opened a new era in experimental fluid mechanics, where physical mechanisms relevant for geophysical questions can be directly and efficiently investigated in laboratory models. In parallel with these advances in digital imaging, the development of alternative techniques as for instance acoustic scattering and instrumented particles, have contributed to this evolution.

Fluid mechanics measurements can be done according to the two traditional approaches : (i) the Eulerian point of view and the Lagrangian point of view. In a Eulerian approach, the fluid velocity is investigated in terms of a spatial field with spatial fluctuations and measurements are done at fixed points $\vec{r}$. Hence in a Eulerian approach, space coordinates $\vec{r}$ are the natural variables to describe the velocity field $\vec{v}_E(\vec{r},t)$ and although this field also experiences in general instantaneous temporal fluctuations, in statistically stationary conditions time t is generally considered as a parameter which helps building ensemble averages by repeating the measurement (if the system is not statistically stationary, then time t becomes a real variable of the problem which accounts for non-stationarity effects). Eulerian measurements have for long been the most widely used in experimental fluid mechanics. This is for instance the case of classical hot-wire measurements as well as PIV (Particle Image Velocimetry) or classical LDV (Laser Doppler Velocimetry). In a Lagrangian approach, instead of probing the flow at given

[1]Laboratoire des Écoulements Géophysiques et Industriels, CNRS/UJF/GINP - Université de Grenoble, BP53 - 38041 Grenoble Cedex 9, France..

[2]J.-F. Pinton, Laboratoire de Physique de l'École Normale Supérieure de Lyon, 46 Allée d'Italie, 69007 Lyon, France.

0148-0227/12/$9.00

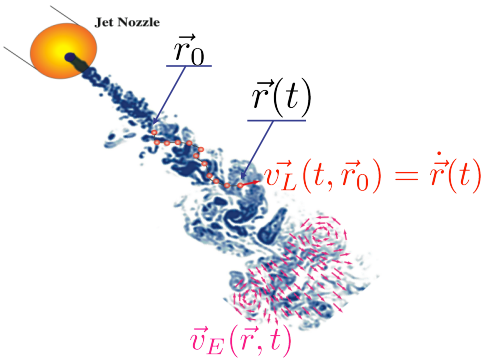

Figure 1. Eulerian versus Lagrangian description of a flow. In the Eulerian framework the flow is described in terms of the velocity field, while in the Lagrangian framework it is characterized from the trajectories of fluid tracers.

fixed points $\vec{r}$ (where fluid particles constantly pass), velocity is measured along the path of given fluid elements which are tagged and tracked individually. In this representation, the natural variable for the velocity fluctuations $\vec{v}_L(t, \vec{r}_0)$ is time t while space coordinates simply parametrize the initial position $\vec{r}_0$ of the tracked fluid particle. In statistically homogeneous conditions, $\vec{r}_0$ is mainly a parameter which is considered either to improve statistical convergence by simultaneously tracking several particles with different initial separations or to address multi-particle problems, as mixing and dispersion.

Eulerian measurements have prevailed in experiment fluid mechanics for decades. Recent progresses in Eulerian measurements mainly concern the improvement of PIV systems, which are now commonly available in 3D-3C configuration (where the three components of the velocity field are measured in a full 3D volume of the flow, for instance using tomographic reconstruction), with an increased repetition rate (thanks to the newest high speed camera technologies) giving access to time resolved measurements.

On the other hand, Lagrangian measurements have known an impressive development in the last years, to the point where Lagrangian particle tracking is nowadays among the most accurate fluid dynamics measurements in terms of spatial ant temporal resolution. Several important factors have contributed to what we can call the *Lagrangian revolution*: (i) the importance of Lagrangian approach has been known for long as Taylor already pointed the relevance of a Lagrangian description of the dynamics of a fluid in the context of mixing and transport phenomena, not to mention dispersion problems which are naturally described in Lagrangian coordinates ; (ii) the investigation of complex flows, such as turbulence for instance, which still resist our comprehension, has motivated new theoretical approaches offering an alternative to usual approaches, such as stochastic models, which are naturally placed in a Lagrangian framework ; (iii) resolved Lagrangian measurements have for long been out of reach in the context of the above mentioned multi-scale problems, due to technological limitations ; the impressive development of high speed digital imaging in the last ten years has finally made it possible to track hundreds of particles simultaneously with sufficient spatial and temporal resolution and to measure for the first time important physical quantities, such as fluid particles acceleration [*Voth et al.*, 2002; *Mordant et al.*, 2001].

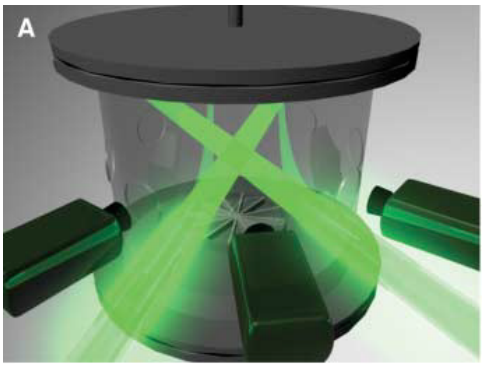

Figure 2. Sketch of a typical 3D-particle tracking experiment. The central part of the bulk of the flow is illuminated using two expanded high power laser beams. Three cameras record simultaneously the motion of small particle tracers in the bulk. (Image taken from [*Bourgoin et al.*, 2006])

In this particular context, we have chosen in this chapter to focus on this *Lagrangian revolution*. We present in the following sections some of the latest measurement techniques applied to state of the art laboratory experiments:

- Optical techniques: Lagrangian tracking and Extended Laser Doppler Velocimetry (ELDV)
- Acoustical techniques: Lagrangian tracking and vorticity measurement
- Instrumented particles.

2. Optical techniques

2.1. Particle tracking

An important advance in Lagrangian measurements has been done in 1997 by Virant and Dracos [*Virant and Dracos*, 1997] who developed a 3D-Particle Tracking Velocimetry (PTV) technique based on the direct imaging of small particles seeding the flow. They used simultaneously 4 video cameras at a frame rate of 25 fps to access the 3D trajectories of several hundreds of particles at once. Ott and Mann [*Ott and Mann*, 2000] developed a similar technique to study relative dispersion of fluid particles. In those two pioneering experiments, because of the low frame rate, particle dynamics could be resolved only for flows at moderate Reynolds numbers ($Re < 4000$ typically). LaPorta *et al.* [*LaPorta et al.*, 2001], used silicon strip detectors (initially developed for high energy particles detection) at a frame rate up to 70kHz, allowing the first fully resolved Lagrangian optical tracking measurements at Reynolds numbers approaching 10^5. However, only one particle at a time could be tracked with the silicon strips. More recently, Bourgoin *et al.* [*Bourgoin et al.*, 2006] developed a high resolution 3D-PTV facility similar to that of Virant & Dracos and Ott & Mann, but using ultrafast cameras at a repetition rate of 27kHz, allowing the tracking of several hundred of particles in high Reynolds number regimes. We present in the following how such a multi-camera tracking system works.

2.1.1. Principle

The principle of optical particle tracking is conceptually very simple: it consists in filming the motion of particles in a flow and to reconstruct their trajectories. However, its practical implementation is a challenge, and several aspects must be carefully considered:

• **Resolution issues.** For high resolution measurements, high speed cameras with a large number of pixels are required. As already discussed, three decades of temporal resolution requires a repetition rate of at least 1 kHz (assuming large structures evolve with a typical time scale around 1 second), while four decades of spatial resolution would in principle require a sensor with at least $10^4 \times 10^4$ pixels. State of the art high speed cameras are typically capable to record $10^3 \times 10^3$ pixel images at several thousands of frame per second, which yields over three decades in time and three decades in space. In practice, as discussed later, experimental noise generally requires to severely oversample the data, and this lowers the time resolution. On the other hand several cameras are generally used simultaneously (as discussed below), which has the additional benefit to improve the effective resolution to about 1/10th of a pixel, hence recovering 4 decades of effective spatial resolution. Resolution is generally a trade-off between temporal and spatial resolution, as higher repetition rates can be achieved by reducing the number of pixels and *vice versa*. However, thanks to the impressive progress in high speed digital imaging technology, direct optical tracking has become one of the most accurate techniques in experimental fluid mechanics

• **3D-measurements.** Complex flows generally involve 3D-structures which require tracking to be done in 3D. This has two consequences: (i) the flow has to be illuminated in volume (a laser sheet, as done for instance in PIV, is not sufficient) and (ii) particles must be tracked in 3D, hence requiring a stereoscopic configuration. In terms of illumination, as the tracers to be tracked are generally small (hence the diffused light is dim), and the repetition rate is high (hence exposure time is short) and the light beam is enlarged (to illuminate a volume), high power light sources are required. High power lasers have been generally used [*Voth et al.*, 2002; *LaPorta et al.*, 2001; *Bourgoin et al.*, 2006], though alternative and less expensive solutions using high power LEDs start to be developed [*Del Castello and Clercx*, 2011]. In terms of recording, the stereoscopic reconstruction requires at least two cameras with two different angles of view to be used simultaneously. In practice three or more cameras are used. Increasing the number of cameras has two main advantages: (i) it allows to track more particles simultaneously, which is interesting to improve statistical convergence of the measurements, specially when multi-particle problems (for instance related to dispersion issues) are investigated ; (ii) the redundancy for particles which are seen simultaneously by more than two cameras, improves the accuracy of the 3D-positionning of those particles, thus leading to an enhanced effective resolution. State of the art optical Lagrangian systems using three or four high speed cameras are capable of tracking several hundreds of particles with 1/10th of pixel of effective resolution. Figure 2 shows the three high speed cameras system implemented by Bourgoin *et al.* [*Bourgoin et al.*, 2006].

• **Data management.** High speed imaging experiments result in a huge data rate. For instance 1 kHz acquisitions with three one megapixel sensors recording at a bit-depth of 8bits, represent an effective data rate of a few Gygabytes per second of recording. These usually requires to couple the acquisition system to dedicated data storage and data processing servers.

The following subsection details the different steps of the data processing which are crucial to warranty the highest possible accuracy of the 3D tracking.

2.1.2. Reconstruction of 3D trajectories

Once the images of the tracers are recorded, the goal is to reconstruct the 3D trajectories of as many particles as possible. This operation consists of three steps:

1. Particle detection: each image (at each time t) of each camera is analyzed to detect and determine the position of the center of each visible particle. This step results in maps of the 2D position of the center of the particles on each frame of each camera.

2. 3D matching: the second step consists in combining at each given time t, the previous 2D maps of particle centers from the N cameras in order to reconstruct (by stereomatching) the 3D position of the center of the particles, with the highest possible accuracy.

3. Lagrangian tracking: finally, once the 3D positions of particles are found for all time steps, an appropriate tracking algorithm allows to reconnect the trajectories.

We describe briefly the key points of the previous steps in the following paragraph. More details and useful information can be found in [*Ouellette et al.*, 2005].

2.1.2.1. Particle detection

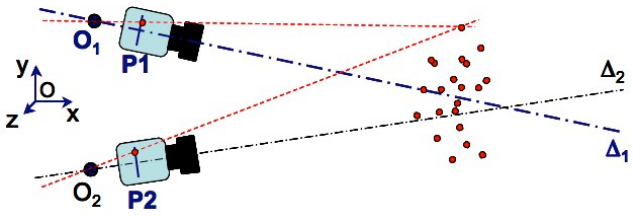

Figure 3.

Ouellette *et al.* [*Ouellette et al.*, 2005] have tested different algorithms for the detection of particle centers on 2D images. The choice of the best algorithm is a compromise between computation time and quality of the detection. The latter is quantified by both the accuracy with which the position of the center of the particles is determined and the number of particles correctly detected. The first step is to identify the local maxima of intensity on the image, indicating the presence of a particle. Then, the image around each maximum is analyzed to determine to the best accuracy the location of the center of the particle. For small particles (as generally used to seed the flow with tracers), the image does not exceed a few pixels. Under these conditions, simple algorithms based on the center of mass of intensity around the maximum are not sufficiently accurate. Algorithms based on neural networks can be very accurate, especially when images are very noisy, but relatively slow. A good compromise consists in fitting the local intensity profile by two gaussians (one vertical and one horizontal), whose maxima define the center of the particle. The choice of two 1D gaussian fits is preferred to that of one single 2D Gaussian because it is computationally significantly more efficient for almost the same accuracy. Ouellette *et al.* have shown that this method was typically capable of detecting 95% of particles and to determine their position with subpixel accuracy.

2.1.2.2. 3D matching

While the detection of particles can be made in the image space of each camera, 3D positioning and Lagrangian tracking Lagrangian must be made in real space (which is common to all cameras). The most widely used method to define the transformation for each camera between image space (in pixels) to real space (in real units), is based on a calibration method developed by Tsai [*Tsai*, 1987]. Each camera (let say we consider camera $\#i$) is represented by a projection model defined by an optical axis Δ_i, an optical center O_i and a projection plane P_i .The image of a particle X on the sensor of camera $\#i$ is then simply given by the intersection of the line O_iX with the plane P_i (see figure 3). The model is generally defined by at least 9 parameters for each camera: 6 external parameters for the absolute position of each camera (3 coordinates for O_i and 3 angles for the orientation of the optical axis Δ_i) and 3 internal parameters (the distance O_iP_i, a coefficient for geometrical aberrations and the aspect ratio of the pixels). Refinement of this basic model can be considered, for instance by including several aberration coefficients (transverse and longitudinal). The parameters of the model are determined from the images of a calibration mask with known geometrical properties. Once the parameters of the model for each camera are determined, the 3D matching is performed as follows (see the illustration in figure 3): take the center of a particle x_i as previously determined in pixels on the projection plane one of the cameras ; the real position X_i of the particle in real space then lies somewhere of the line of view O_ix_i. The

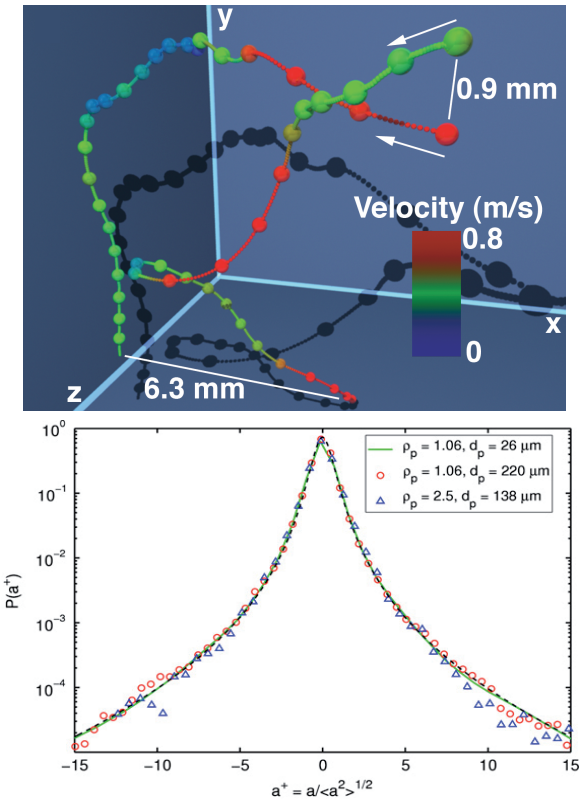

Figure 4. Top: Example of high resolution reconstruction of particle trajectories in experiment shown in figure 2. The small spheres mark every other measured position of the particles and are separated by 0.074 ms ; the large spheres mark every 30th position. Color indicate the velocity of the particle along its trajectory. (Figure from [*Bourgoin et al.*, 2006]). One component acceleration statistics measured in a von Kármán swirling flow seeded with particles of different size and density (figure from [*Xu and Bodenschatz*, 2008])

intersection of such line of views from two (or more) cameras defines the absolute 3D position of the particle in real space. In theory two cameras are sufficient to determine this intersection. In practice however, the lines of view rarely intersect due to slight imprecision in the calibration of the Tsai model. The 3D position is then defined as the point in real space which minimizes the distance to the different lines of view. Whenever a camera is added in the system, the redundancy of information provided by the additional line of view further restricts the possible 3D position of the particle. This greatly improves the effective spatial resolution 3D system. Ouellete *et al.* have shown that using three cameras instead of two gives an effective resolution of the order of one tenth "equivalent pixel" (that is to say one tenth of the spatial dimension whose image is the size of a pixel taking into account the magnification of the projection system). Thus the combination of three sensors of $10^3 \times 10^3$ pixels provides an effective spatial resolution of 4 decades in 3D. Adding a fourth camera, is then essentially interesting to increase the number of particles actually followed. Indeed, ambiguous situations where a particle hides another one in the line of sight of a camera may occur. These ambiguities can be lifted by adding a fourth camera at a different angle, in order to maximize the number of particles which are seen at any time by at least three cameras.

2.1.2.3. Trajectory reconnections

Lagrangian tracking consists in reconnecting particle trajectories between successive time steps. This requires to identify at time $t+1$ particles already detected at time t. Lagrangian tracking algorithms are generally based on the minimization of a given cost function. The simplest algorithm, called *nearest neighbour* simply consists in connecting a particle (let say particle $\#j$) whose position at time $t+1$ is $\vec{x}_j(t+1)$ to the particle $\#i$ whose position at time t minimizes the cost function $\phi_{ij} = \| \vec{x}_i(t) - \vec{x}_j(t+1) \|$. This simple algorithm is accurate only if the inter frame displacement is significantly less than the average inter particle separation. It is therefore generally limited to relatively diluted configurations. In higher seeding density situations, more sophisticated algorithms are required. As shown by Ouellette *et al.*, one robust algorithm consists in defining a cost function ϕ_{ij} based on four consecutive images. Qualitatively, it is based on a smoothest acceleration criterion. Quantitatively it is implemented as follows: assume trajectories has been reconnected up to time step t ; the velocity of the particles is estimated from positions $\vec{x}_i(t)$ and $\vec{x}_i(t-1)$, what allows to estimate their probable position at time $t+1$, $\tilde{\vec{x}}_i(t+1)$; then particle acceleration is estimated from $\vec{x}_i(t-1)$, $\vec{x}_i(t)$ and $\tilde{\vec{x}}_i(t+1)$, what allows to propagate at time $t+2$ an estimation $\tilde{\vec{x}}_i(t+2)$ of the position for each particle in the vicinity

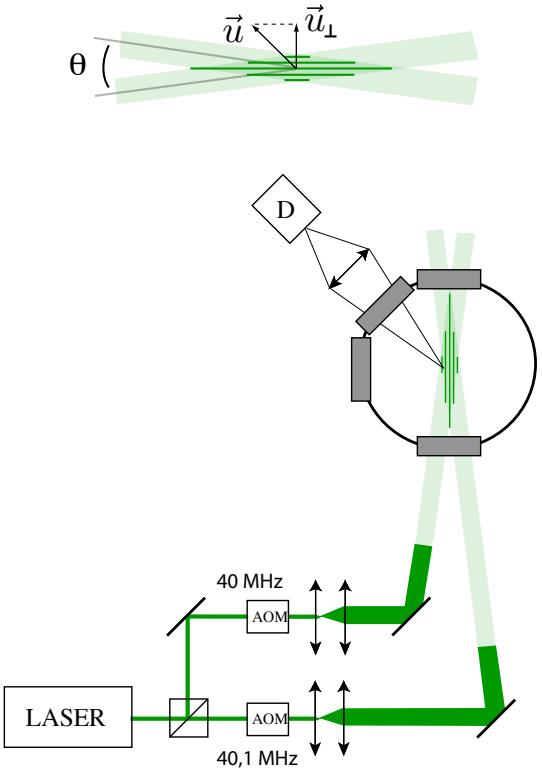

Figure 5. Optical arrangement of Extended Laser Doppler Velocimetry detailed in [*Volk et al.*, 2008, 2010]. Two laser beams (with wavelength λ_0) forming an angle θ intersect to create an interference pattern with fringe spacing $a = \lambda_0/(2\sin(\theta/2))$. Each beam is shifted in frequency with an Acousto Optic Modulator and Expended using a telescope. The measurement volume is imaged onto a photodetector using a lense. A particle crossing the fringes scatters light modulated at frequency $f_p(t) = \delta f + u_\perp(t)/a$ with δf the frequency shift between the beams and $u_\perp(t)$ the component of velocity perpendicular to the fringes.

of $\vec{\tilde{x}}_i(t+1)$; then the most probable trajectory is that minimizing the cost function $\phi_{ij} = \| \vec{\tilde{x}}_i(t+2) - \vec{x}_j(t+2) \|$.

2.1.3. Example of 3D optical tracking

Figure 4a shows an example of tracking of pairs of particles by Bourgoin *et al.* [*Bourgoin et al.*, 2006] in the high Reynolds number experiment previously shown in figure 2. The figure only shows two trajectories, but hundreds of such trajectories are simultaneously reconstructed. This allows a rapid statistical convergence of particle displacement, velocity and acceleration statistics. Such data can be used to investigate different properties of the flow. In the study by Bourgoin *et al.* separation statistics are investigated in order to address the longstanding question of turbulent super diffusion. But time resolved trajectories can be differentiated with time, once to obtain particle velocity and twice to access particle acceleration. Optical tracking of small particles has shown the highly intermittent dynamics of such fluid tracers in turbulent flows. This is revealed for instance by measurements of acceleration statistics in von Kármán swirling flows (shown in figure 4b) which exhibit highly non-gaussian fluctuations corresponding to events of very high acceleration occurring with a probability orders of magnitude larger than what would be expected for a normal random process with equivalent variance.

2.2. Extended Laser Doppler Velocimetry

As already mentioned, particle tracking is very demanding in terms of acquisition frequency which needs to be much larger than the inverse of the Kolmogorov timescale $1/\tau_\eta = \sqrt{\epsilon/\nu}$ with a spatial resolution comparable with the Kolmogorov scale $\eta = \left(\nu^3/\epsilon\right)^{1/4}$ in order to access the very small scales of the particles motion. For typical water flows at the Lab scale one therefore needs to track particles with sizes in the range $10-100$ microns with a sampling frequency larger than several kilohertz, which is a severe limitation in terms of camera specifications and cost of the experiment. To increase the temporal resolution at a modest cost, one possibility is to rely on scattering techniques using a reference wave (either using ultrasound or Laser light) that will be scattered by the moving particles. This is the basis of the so-called Laser Doppler Velocimetry (an Eulerian measurement technique), and of Extended Laser Doppler Velocimetry which is its extension to Lagrangian measurements.

Principle of Laser Doppler Velocimetry. The principle of Laser Doppler Velocimetry is very simple: it uses two coherent laser beams (with wavelength λ_0) intersecting with an angle θ to create an interference pattern consisting in fringes perpendicular to the plane of the beams laser beams, separated by a distance $a = \lambda_0/(2\sin(\theta/2))$. When a particle crosses the fringes, it scatters light with an intensity $I(t)$ modulated with a frequency $f_p = u_\perp/a$, were $u_\perp$ is the component of velocity perpendicular to the fringes (figure). If the measurement volume (region were the beams intersect) extends over a large region of space, a continuous detection of the instantaneous frequency $f_p(t)$ gives access to the evolution of the particle's velocity as a function of time. Such an Extended Laser Doppler Velocimetry was developed by Volk and coworkers [*Volk et al.*, 2008, 2010] to perform velocity tracking of small particles in high Reynolds number flows.

Optical arrangement. To obtain interference fringes in a large portion of space, only one Laser beam is used: it is separated by a beam-splitter into two coherent beams separately expanded using two pairs of lenses as telescopes. In order to get the velocity sign, the common technique consists in shifting the modulated optical signal by a frequency δf so that the actual modulation is at frequency $f_p(t) = \delta f + u_\perp(t)/a$. This is achieved by propagating the two beams through Acousto-Optic Modulators (AOM) with frequency shifts $f_1 = 40$ MHz and $f_2 = 40.1$ MHz so that the fringes are actually moving at constant velocity $v_f = a(f_2 - f_1) = a \cdot \delta f$.

Particle detection. In practice, the intensity needed for the measurement depends on the particles used as tracers of the flow motion. Using a 1 W continuous Argon laser of wavelength 514 nm and a small angle between the beams, one can obtain a fringe spacing $a = 41$ μm. This is much larger than in classical LDV applications and allows for the use of polystyrene fluorescent (with size 30 microns) or larger non fluorescent particles. For the fluorescent particles case, scattered light is weaker and the measurement volume has to be imaged on a low noise photomultiplier with high gain. For particles larger than 100 microns, scattered signal is stronger and the detection can be made using amplified photodiodes with less than 0.5 W of Laser power. As opposed to fluorescent particles, the optical contrast of the scattered signal strongly depends on the photodetector location and particle size, the detector is placed in the plane of the beams, in front face configuration at 45 degrees from the beams.

Signal acquisition. The use of two AOM instead of one (for classical LDV) allows for a small frequency shift 100 kHz so that raw data can be acquired using high speed DACQ. Each time a particle crosses the measurement volume, it produces a burst of light with signal of the form (figure 6(a)) :

$$s(t) = \alpha(t) + \beta(t)\cos(2\pi\delta f \cdot t + \phi(t)), \quad (1)$$

$$\text{with} \quad \frac{d\phi(t)}{dt} = 2\pi\frac{u_\perp(t)}{a} \quad (2)$$

where $\alpha(t)$ and $\beta(t)$ are slowly varying envelopes originating from the Gaussian radial profiles of the beams. When the scattering intensity exceeds a prescribed threshold the signal is recorded and stored for post processing on a PC. In typical situation the diameter of the beams d is much larger than the fringe spacing a so that there is a scale separation

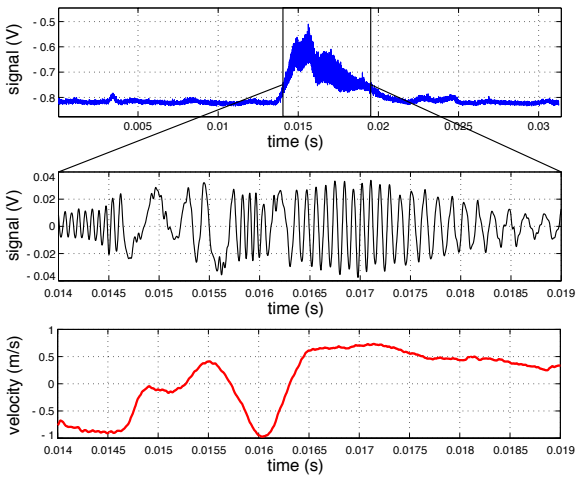

Figure 6. Typical optical signal measured with Extended Laser Doppler Velocimetry. Up : burst observed when a particle crosses the measurement volume. Middle : real part of the complex signal obtained signal after filtering and demodulation from carrying frequency $\delta f = 100$ kHz. Down : corresponding evolution of velocity as obtained from parametric estimation.

between the fast modulation at frequency $f(t) = u_\perp(t)/a$ and the slow amplitude modulations $\alpha(t)$ and $\beta(t)$.

Signal processing. After running the experiment, the velocity is computed from the collection of light scattering signals $(s_i(t))_{[1,N]}$. This signal processing step is crucial as both time and frequency – *i.e.* velocity – resolutions rely on its performance. As the local frequency of the signal is varying in time, common time-frequency techniques based on Fourier analysis [*Flandrin*, 1998] (such as *short time Fourier transform* are usually too limited as the Heisenberg principle imposes that $\delta_t\delta_\nu > 1i$, what means that one cannot have both high resolution in time (which is crucial to resolve the fastest dynamics of the particles) and frequency (which is crucial to have a good measurement of particles velocity, which according to relation (2) is directly given by $\delta_n u$). It is therefore necessary to overpass Heisenberg principle limitation. Several methods exist, including Cohen class energetic estimators (such as Wigner-Ville and Choï Willians distributions) [*Flandrin*, 1998] which can be further refined using the *reallocation* technique [*Flandrin*, 1998; *Kodera et al.*, 1976]. These methods are relatively time consuming in terms of computational processing, and are generally adapted for situations where no information is *a priori* known on the form of the signal to be analyzed.

In order to increase the frequency resolution with small observation window Mordant and coworkers introduced a fast demodulation algorithm with parametric estimation [*Mordant et al.*, 2002, 2005]. It relies on a comparison between the measured signals $(s_i(t))$ and model given in equation (2). In practice, such a parametric estimate of amplitude and frequency modulations are very robust with respect to the unavoidable experimental noise. The estimation is done in several steps :

1. As the timescale of $\alpha(t)$ (of order $d/u \sim 5$ ms) is very large as compared to $1/\delta f = 0.01$ ms, it is removed with high pass filtering at several kiloHertz.

2. To obtain an absolute definition of the local frequency through the evolution of the phase $\phi(t)$, the filtered signal $s'(t)$ is transformed into an analytical complex signal $\underline{x}(t)$: this is done using the Hilbert transform $\mathrm{HT}[s'](t)$ of the measured signal with the definition $\underline{x}(t) = s'(t)+i\mathrm{HT}[s'](t)$. The amplitude and frequency of the signal are then $\alpha(t) = \|\underline{x}(t)\|$ and $f_p(t) = \delta f + d\phi/dt$.

3. The complex signal $\underline{x}(t)$ is then demodulated from the carrying frequency by multiplication by $\exp(-2i\pi\delta f\cdot t)$. The real part of such demodulated complex signal for a typical burst is displayed in figure 6(middle).

4. To perform a fast and precise measurement of the modulation frequency, an approximated maximum likelihood (AML) method is coupled with a Kalman filter to perform a parametric estimation of the instantaneous amplitude and frequency. In a moving window of duration δT, centered at time t, it assumes that the signal is made of a modulated complex exponential plus Gaussian noise $n(t)$, and compares the measured signal $\underline{x}(t)$ to the functional form

$$\underline{z}(t) = A(t)e^{i2\pi\int_0^t \nu(t')\mathrm{d}t'+i\psi} + n(t), \qquad (3)$$

were $A(t)$ and $\nu(t)$ are the unknown amplitude and frequency to be estimated and ψ a constant phase originating from the initial particle position in the measurement volume. As an output, one obtains for each trajectory an estimate of the frequency $\nu(t) = u_\perp(t)/a$, amplitude $A(t)$, plus a confidence criterion $h(t)$ which measures the quality of the estimation at each time step. This is done for each trajectory on a Personal Computer using Matlab to obtain a collection of trajectories to be further used to compute Lagrangian statistics of the flow.

Initially designed for acoustical Doppler measurement, the demodulation technique proved to be fast and accurate enough to perform Lagrangian ELDV measurements with typical time resolution 10 μs and sampling rate 300kHz. This represents the highest sampling rate ever used for Lagrangian measurements in high Reynolds number flows.

Particle seeding issues. For practical applications, the particles seeding density has to be adjusted in order to be low enough so that one does not observe events with two particles at the same time in the measurement volume, but high enough to observe several trajectories per second. For a fully turbulent flow with Reynolds number at Taylor microscale $Re_\lambda \sim 600$, a collection of 15000 trajectories with mean duration 20 Kolmogorov times (τ_η) is enough to converge velocity statistics, acceleration statistics and acceleration autocorrelation function. In the case of acceleration autocorrelation $C_{aa}(\tau) = \langle a(t)a(t+\tau)\rangle/\langle a^2\rangle$, one gets access to an estimate of the local kinetic energy dissipation ϵ because the integral of the positive part of the curve is very close to the dissipation time $\tau_\eta = \sqrt{\nu/\epsilon}$ [*Volk et al.*, 2010]. As shown in figure 7(up), there is a good rescaling between the acceleration autocorrelation functions when time is measured in τ_η units for fully developed turbulent flows of water (with kinematic viscosity 10^{-6} m^2/s and dissipation scale 19 microns) and water-glycerol mixtures (kinematic viscosity $8\cdot10^{-6}$ m^2/s, dissipation scale 90 microns). These

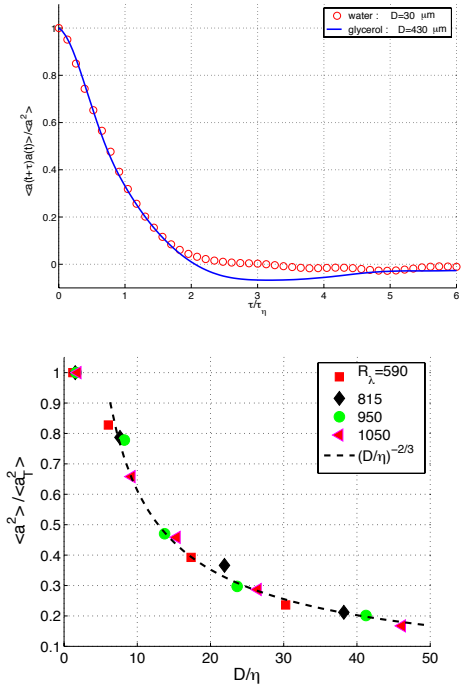

Figure 7. Up : Acceleration autocorrelation function $C_{aa}(\tau) = \langle a(t)a(t+\tau)\rangle/\langle a^2\rangle$ measured with ELDV in a fully developed turbulent flow. For both curves, time has been rescaled by the dissipative time $\tau_\eta = \sqrt{\nu/\epsilon}$. $(\circ)$ 30μm fluorescent tracer particles for a water flow with dissipation scale $\eta = 19\mu$m. $(-)$ large 430μm polystyrene particles behaving as tracers in the same (water-glycerol) flow with dissipation scale $\eta = 90\mu$m. For the two situations, the large scale driving and dissipation $\epsilon = 20$ W/kg are the same. Down : Acceleration variance of particles with size D normalized by the one measured for tracers as a function of the ratio D/η. Particles with size $D/\eta > 5$ no longer behave as tracers of the flow motions.

two curves also show that particles with diameters $D = 5\eta$ (the dissipative scale) can still be considered tracers of the flow movement. As shown in 7(down), this is no longer the case for larger particles for which one observes a decrease of particle acceleration variance following a power law $\langle a_D^2 \rangle / \langle a_{tracer}^2 \rangle \propto (D/\eta)^{-2/3}$. This decrease of acceleration variance goes together with an increase of the particle acceleration autocorrelation time [*Qureshi et al.*, 2007; *Brown et al.*, 2009; *Volk et al.*, 2010].

3. Acoustic techniques

Whenever a sound wave encounters an obstacle or inhomogeneity along its propagation path, it is deflected from its original course, a phenomenon called acoustic scattering. The scatterer can be either a material obstacle or a physical inhomogeneity such as temperature or velocity gradient, which creates a contrast of acoustic impedance and influences the propagation of sound. The properties of the scattered acoustic wave depends upon the frequency of incident wave, the shape and size of the obstacles as well as their velocity. It is possible to take advantage of these scattering properties to probe the dynamics of fluids. We present here two important techniques based on acoustic scattering : (i) Lagrangian acoustic tracking, which exploits the Doppler effect shift of the wave scattered by moving particles ; (ii) acoustical measurements of vorticity, which exploits the scattering properties of eddies in a fluid (with no need of seeding the flow). Note that these techniques are intrinsically related to acoustic scattering properties and differ from other classical acoustic techniques based on echoing and measurements of time of flight of acoustic bursts.

3.1. Acoustic Doppler Lagrangian tracking

3.1.1. Principle

Acoustic Lagrangian tracking is based on the measurement of the Doppler shift of the acoustic wave scattered by a moving particle. Figure 8 (top) presents the principle of one-component ultrasonic Doppler velocimetry. An acoustic transducer emits a continuous ultrasonic wave at a given frequency ν_0 with a propagating direction $\vec{n}_0$. Whenever a particle crosses the acoustic beam of the emitter, it scatters the acoustic wave. An acoustic receiver then listens to the scattered wave in a specifc direction $\vec{n}_s$ ($\theta_s = (\vec{n}_0; \vec{n}_s)$ is the scatter angle). The intersection between the emitting and the receiving beams defines the measurement volume, where particles can be actually detected. Because the particles moves, the scattered wave is Doppler shifted an its frequency ν_s differs from ν_0 so that

$$\frac{\nu_s - \nu_0}{\nu_0} = \frac{\vec{V} \cdot (\vec{n_0} - \vec{n_s})}{c} = -2\frac{v_{//}}{c} \sin(\theta_s/2), \qquad (4)$$

where c is the speed of sound in the experimental conditions. For a given incident frequency ν_0 and a given scatter angle θ_s, the instantaneaous frequency shift $\delta\nu(t) = \nu_s - \nu_0$ gives a direct measurement of the projection, $v_{//}$, of the particle velocity along $\vec{n}_0 - \vec{n}_s$ (note that this is an algebraic measurement : the sign of $v_{//}$ is given by the sign of the frequency shift). Hence, the continuous recording of the frequency shift $\delta\nu(t)$ gives a Lagrangian measurement of the velocity component $v_{//}(t)$ along the particles trajectory. It is interesting to note the analogy of this acoustic technique with the optical ELDV method previously described. The modulation of scattered light by a particle moving in the interference pattern in ELDV is indeed conceptually equivalent to the modulation of the Doppler shifted acoustic wave scattered by a particle in the present configuration. Finally, we point that the combination of several pairs of transducers and working frequencies allows to extend the measurement

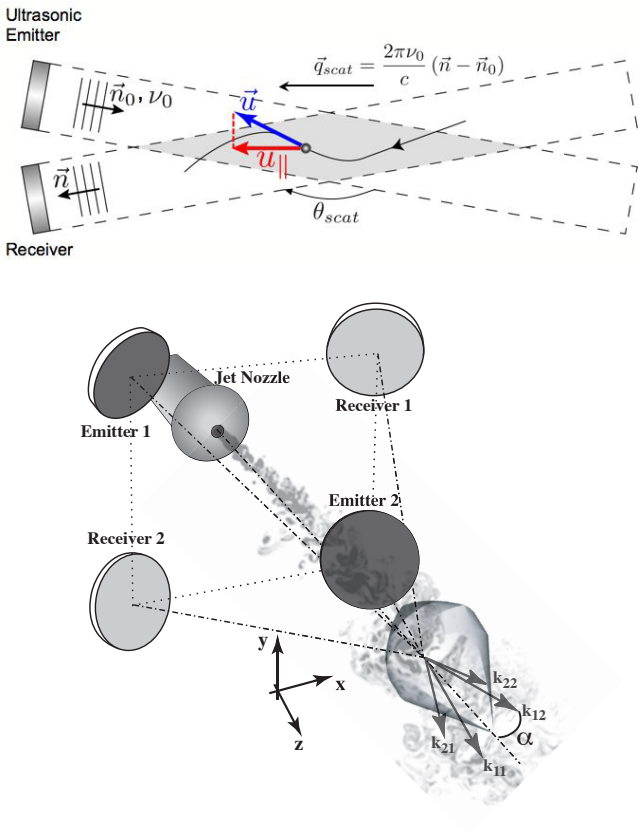

Figure 8. Top: Principle of one-component acoustic Doppler velocimetry. Note the analogy with the optical system presented for the ELDV (see figure 2.2). Bottom: Example of transducer arrangement for the acoustic Lagrangian tracking of the three component of the velocity. Four transducers (two emitters and two receivers) are placed at the vertices of a square, tilted so that their axes cross at the same point on the jet axis, in a square-based pyramid configuration. The two emitter operate at two different working frequencies $\nu_{0,1}$ and $\nu_{0,2}$ and receivers listen to scattered waves in the vicinity of each of this frequencies.This arrangement is this composed of four independent pairs of emitter-receiver capable of measuring four projections of the velocity, which gives a redundant 3D measurement, where redundancy improves the signal to noise ratio (SNR). Adding extra transducers would increase further the SNR.

and access two or three components of the velocity (see Figure 8 (bottom)).

Such an acoustic Lagrangian tracking technique was first implemented by Mordant *et al* [*Mordant et al.*, 2002, 2001, 2005] in a pioneering study of Lagrangian turbulent statistics in a von Kármán swirling flow of water. In that case, piezo-electric elements were used as acoustic transducers (with typical emitting frequency operating in the MHz range) and small polystyrene particles served as tracers. More recently, the same technique was ported to investigate opened air flows in a turbulent jet [*Poulain et al.*, 2004] and wind-tunnel experiments [*Qureshi et al.*, 2007, 2008] ; the same system can also be easily ported to *in situ* measurements in real atmospheric flows. In these experiments Sell type acoustic transducers were used, operated with typical frequencies around 100kHz (ultrasounds at higher frequency are rapidly damped in air) and tracked particles were small milimmetric soap bubbles either neu-

trally buoyant (bubbles are then inflated with Helium) to have tracer behavior or intentionally heavier than air in order to address the question of the turbulent transport of inertial particles.

Pros and cons of scattering techniques compared to direct optical methods can be discussed. The main advantage of acoustics is that Doppler shift measurements give a direct access to the tracer's velocity, while optical tracking requires to differentiate the position signal of the tracked particle to get velocity, an operation which is very sensitive to noise. Hence optical tracking usually requires severe oversampling if velocity and acceleration statistics are to be investigated. Other advantages of acoustic tracking concern (i) the low cost of the required equipment, compared to expensive high speed cameras, (ii) the possibility to easily explore large volumes, (iii) to investigate open flows with large mean velocities and (iv) to probe flows in opaque fluids (as liquid metals for instance). The last point is particularly important for instance in wind-tunnel or jet experiments where efficient optical tracking generally requires to mount the camera on a platform moving at the mean wind speed [*Ayyalasomayajula et al.*, 2006] in order to track particles for sufficiently long times (typically comparable to the largest time scales of the flow) while, acoustic tracking can be efficiently done using fixed transducers ; moreover a backscattering configuration ($\theta_{scatt} \lesssim 180°$) allows to significantly extend the streamwise dimension of the measurement volume [*Qureshi et al.*, 2007, 2008].

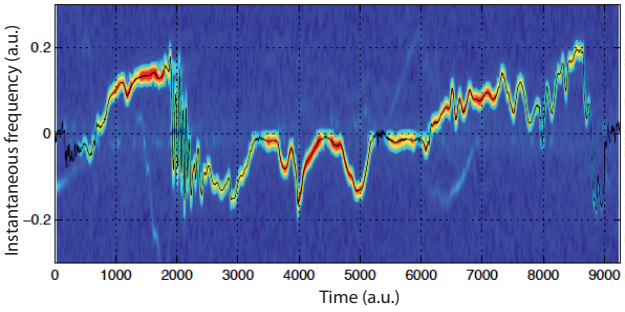

Figure 12. Example of reconstruction of the instantaneous frequency scattered by a moving sphere in a swirling flow of water. The color image represents the spectrogram computed with usual Fourier analysis time-frequency analysis (the width of the frequency trace illustrates the incertitude due to Heisenberg constrain) to which is superimposed the estimation given by the AML method (solid black line). (Image taken from [*Mordant*, 2001].)

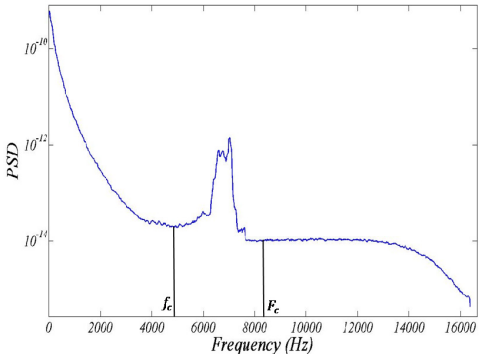

Figure 10. Typical spectrum of the donwmixed acoustic signal recorded by the receiver. The Doppler shift resulting from the scattering by moving tracers is visible around 7 kHz (image taken from [*Qureshi*, 2009]).

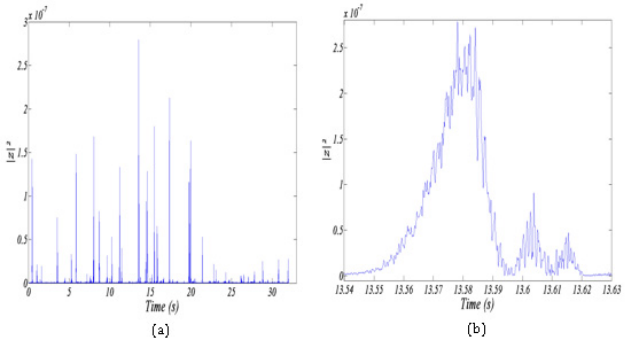

Figure 11. (a) Typical amplitude of the recorded down-mixed signal bandpass filtered around the Doppler peak (between frequencies f_c and F_c as shown in figure 10). Peaks of high amplitude correspond to events where a particle travels into the measurement volume and scatters the incident acoustic wave towards the receiver. (b) Zoom on one such isolated event. (image taken from [*Qureshi*, 2009]).

On the cons side, a strong limitation of acoustic tracking is its inability to accurately track several particles simultaneously. If more than one particle is present in the measurement volume, the signal recorded by the receiver superimposes the waves scattered by all the particles. Although signal processing strategies (discussed below) do exist to extract the contributions from each individual scatterer the accuracy decreases with increasing number of particles.

3.1.2. Signal Processing and doppler shift extraction

The acoustic signal recorded by the receiver combines a spectral component around the emitting frequency ν_0, which corresponds to echoes and reflections directly incoming in the receiver without being scattered by the particles and a Doppler shifted component around ν_d resulting from the fraction of acoustic wave scattered by the moving particle. The sought information, on particles velocity, is entirely encoded in the Doppler shift $\delta_\nu = \nu_d - \nu_0$. Therefore, a heterodyne downmixing is generally operated between the emitted and received signal what essentially results in shifting the emitting frequency ν_0 to zero. Figure 10 shows a typical spectrum of a downmixed signal recorded in the wind-tunnel experiment by Qureshi *et al.* [*Qureshi et al.*, 2007]. The peak at zero frequency corresponds to the emitting frequency ν_0 (which was 80 kHz in this experiment) and the secondary peak (around 7 kHz) corresponds to the Doppler shift from the wave scattered by moving tracers (note that the central peak at the emitting frequency is enlarged by aerodynamic effects). The interest of heterodyne down mixing is that recording the original signal would require very high sampling rates, as the Doppler frequency would be here around $\nu_d = \nu_0 + \delta_n u \simeq 87$ kHZ), while it is only at 7 kHz after downmixing.

Figure 11(a), shows the amplitude $A(t)$ of the downmixed signal, whose spectrum was previously discussed, versus time; each peak of amplitude corresponds to the passage of a particle in the measurement zone. The spectrum previously discussed was calculated from the entire times series and hence all time information has been lost: the observed

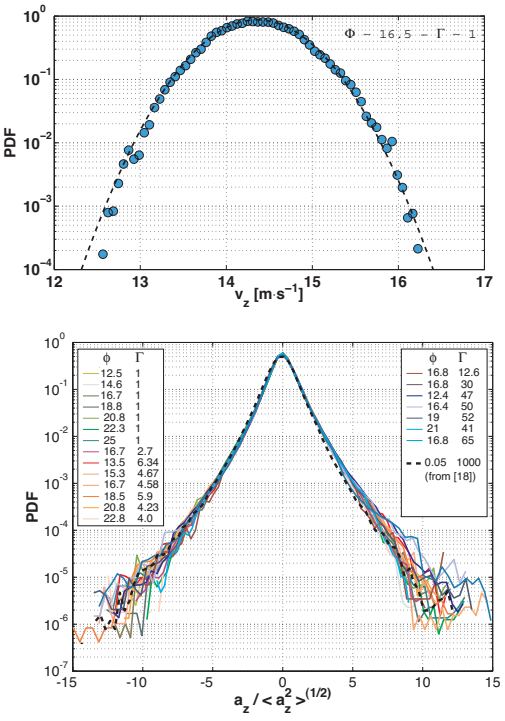

Figure 13. Top: One component Lagrangian velocity PDF of finized particles neutrally buoyant particles transported in a turbulent wind-tunnel flow (Image taken from [*Bourgoin et al.*, 2011]). Bottom: Acceleration PDF of finite size material particles with different sizes and density in the same wind-tunnel flow (Image from [*Qureshi et al.*, 2008]).

Doppler peak corresponds to the superposition of spectral contributions from thousands of successive scattered traveling through the measurement volume. It is only interesting to extract global informations, such as the average velocity of the particles (given by central frequency of the Doppler peak) or the typical level of velocity fluctuation (given by the width of the Doppler peak). However, accessing the Lagrangian dynamics of the particles requires to extract the instantaneous Doppler shift $\delta_\nu(t)$ for each individual particle.

This is achieved in two steps: first, each event corresponding to the passage of a particle is detected from the amplitude signal as shown in figure 11(a) (figure 11(b) shows a zoom on such an individual particle event ; second, the portion of signal corresponding to each individual event is analyzed with dedicated time-frequency tools to extract the instantaneous Doppler shift. For the same reasons previously discussed in the context of optical ELDV, the instantaneous Doppler shift can be efficiently extracted using a maximum of likelihood algorithm where after down-mixing, the signal scattered by one particle and recorded by the receiver is modeled with the following form :

$$z_i(t) = A_i(t) e^{i2\pi \int_0^t \delta\nu_i(t')\mathrm{d}t'} + n(t) \qquad (5)$$

where $A_i(t)$ is the amplitude of the scattered acoustic wave, $\delta\nu_i(t)$ is the instantaneous frequency of the signal (subscript i indicates that we consider particle number i) and $n(t)$ represents an additive experimental noise. The AML algorithm determines for each particle i the best functions $A_i(t)$ and $\delta\nu_i(t)$ so that the model given by eq. 8 matches as close as possible the actual recorded signal ($n(t)$ is assumed to be a random gaussian noise whose amplitude is fixed according the actual noise level of the experimental signal. Such a parametric algorithm is capable of overcoming the Heisenberg limitation (which would severely constrain the resolution of the measurement), thanks to the extra information (given by the *a priori* imposed shape of the signal in eq. (8) added in the signal processing. The gain in resolution offered by the AML method is illustrated by figure 12. Also of interest is the fact that the AML algorithm gives a quantitative indicator of the relevance of the expression (8) to actually model the recorded signal. This allows for instance to discard from the statistical ensemble events where for instance two particles were simultaneously present in the measurement volume which would require a more sophisticated model (situations with n particles can be a priori model as a linear superposition of the previous expression : $z(t) = \sum_{i=1}^{N} z_i(t)$).

3.1.3. Example of acoustical particle tracking

Acoustical tracking has been used in different experimental facilities, including von Kármán swirling flows, turbulent jets and wind-tunnels to investigate both the characteristics of the flow and the dynamics of material particles transported by the flow. Figure 13 represents the probability density functions of the velocity and acceleration of material particles transported in a turbulent wind-tunnel flow. Velocity is found to have gaussian statistics while acceleration exhibit wide non-gaussian tails, even for particles much denser than the fluid.

3.2. Vorticity measurements

Measuring vorticity of a flow has always been a challenge in experimental fluid mechanics, especially when small scales are to be probed. We recall that the vorticity $\vec{\Omega}$ of a velocity field $\vec{u}$ is given by the curl of $\vec{u}$ ($\vec{\Omega} = \vec{\nabla} \times \vec{u}$). A direct measurement of vorticity is usually achieved from spatial derivatives of the velocity field. This is typically achieved for instance from PIV measurements of the velocity field or from complex multiple hot-wire probes. However, in either cases, the spatial resolution is an issue when flows are highly turbulent as neither PIV, nor multiple hot-wire probes are capable of resolving the smallest dissipative scales of the velocity fields, what is required to accurately estimate velocity spatial derivatives. We present in this section an elegant measurement of the vorticity of a flow based on the interaction between an acoustic wave and the structures of the flow.

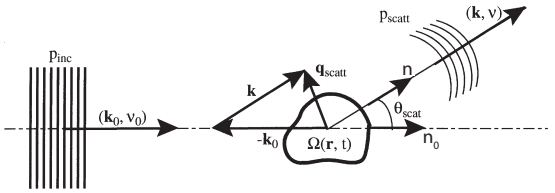

Figure 9. Typical implementation of acoustic scattering for probing the vorticity field of a flow. An ultrasonic emitter generates a plane acoustic wave in the direction $\vec{n}$ at the frequency ν_0. A receiver listen to the acoustic wave scattered in a given direction $\vec{r}$. The relative amplitude of the scattered acoustic pressure to the incident acoustic pressure can be related to the spectral distribution of the vorticity field $\vec{\Omega}(\vec{x}, t)$ according to relation 6.(Image taken from [*Poulain et al.*, 2004].)

3.2.1. Principle

Acoustical measurement of vorticity is based on the scattering of an acoustic wave by the velocity gradients of the

flow. The scattering properties from this acoustic-fluid interaction are non-trivial. Several theoretical and numerical studies can be found on the subject [*Obukhov*, 1953; *Kraichnan*, 1953; *Chu*, 1958; *Batchelor*, 1957; *Lund and Rojas*, 1989; *Llewellyn Smith and Fort*, 2001; *Colonius et al.*, 1994]. In particular, using a Born approximation, Lund [*Lund and Rojas*, 1989] has shown that the scattered amplitude of a plane acoustic wave by a turbulent flow can be linearly related to the spatial Fourier transform of the vorticity field of the flow. This property can be qualitatively understood as the fact that each vortex in the flow acts as a scatterer which radiates a sound wave as it is perturbed by the incident impinging acoustic wave. The global scattered wave, results from the coherent average over the scatterers distribution. Figure 9 illustrates a typical acoustical scattering configuration which can be used to probe the vorticity of a flow.

Lund *et al.* have shown that the acoustic pressure amplitude and the Fourier transform of the vorticity field can be related as follow:

$$p_{\rm scat}\left(\vec{k},t\right) = L(\theta_{\rm scat})\tilde{\Omega}_{\perp}\left(\vec{q}_{\rm scat}=\vec{k}-\vec{k}_0,t\right)p_{\rm inc}\left(\vec{k}_0,t\right) \tag{6}$$

where $\vec{k}_0$ and $\vec{k}$ are the vector wave-numbers of the incoming and scattered acoustic waves respectively, $\theta_{\rm scat}$ is the scattering angle, $p_{\rm inc}$ and $p_{\rm scat}$ are the complex pressure amplitudes of the incoming and scattered acoustic wave respectively, $L(\theta_{\rm scat})$ is an angular factor which will be discussed further below and $\tilde{\Omega}_{\perp}$ is the component of the space Fourier transform of the vorticity perpendicular to the scattering plane defined by the vector wave-numbers of the incident and scattered acoustic waves (see figure 9):

$$\tilde{\Omega}_{\perp}\left(\vec{q},t\right) = \left(\vec{n}_0\times\vec{n}\right)\cdot\int\int\int\vec{\Omega}\left(\vec{r},t\right)e^{-i\vec{q}\cdot\vec{r}}{\rm d}^3\vec{r} \tag{7}$$

Equation (6) therefore shows that the amplitude of the scattered wave gives a direct measurement of one Fourier mode of the vorticity component $\Omega_{\perp}$. Interestingly, the Fourier mode at which the vorticity field is being probed is directly selected by the imposed scattering vector $\vec{q}_{\rm scat} = \vec{k}-\vec{k}_0$. Hence, it is possible to reconstruct the complete vorticity spectra by spanning the explored scattering vector, what can be done either by changing the angular position of the acoustic receiver or by changing the operating acoustic frequency (as $\parallel\vec{q}_{\rm scat}\parallel\simeq 4\pi\nu_0/c\sin(\theta_{\rm scat})$, assuming the Doppler shift $\nu-\nu_0$ remains small compared to ν_0).

It is important to stress that this measurement is local in Fourier space, meaning that for a given scattering vector, only the mode of vorticity at wavenumber $\vec{q}_{\rm scat}$ is actually measured. Hence the measurement is naturally global in space and the corresponding spectral mode is characterized across the entire measurement volume. Though the scattering structures of the flow are tracked as they move across the flow (this results for instance in a Doppler shift of the scattered acoustic wave) the recorded signal represents a coherent average of all structures at the probed scale simultaneously present in the measurement volume and no information is extracted from individual scatterers. As a consequence this technique is not properly speaking of Lagrangian type, although the metrology technique and instrumentation is almost identical to that described in the previous subsection on Lagrangian acoustical tracking.

An important point to be considered is the angular factor $L(\theta_{\rm scat})$. Figure 14 shows the dependency of $L(\theta_{\rm scat})$ with the scattering angle $\theta_{\rm scat}$ as calculated by Lund *et al.*. It shows a quadrupolar like radiation pattern which diverges at zero angle (Borm approximation fails in this limit) and vanishes for scattering angles $\theta_{\rm scat}=90^\circ$ and $\theta_{\rm scat}=180^\circ$

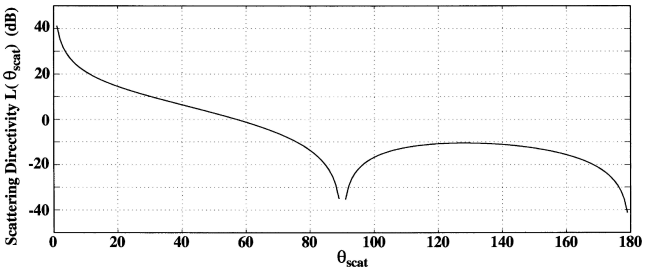

Figure 14. Angular factor $L(\theta_{\rm scat})$. (Image taken from [*Poulain et al.*, 2004].)

(back-scattering situation). Those two specific scattering angles are to be avoided for the vorticity measurement. On the contrary, they are optimal for particle tracking as no signal is then recorded from scattering effects of the fluid itself, and only the particles seeding the flow will be seen. This explains the back-scattering configuration chosen for the acoustical particle tracking described in the previous subsection.

3.2.2. Experimental implementation and typical results

Experimental evidence of ultrasonic scattering by vortical structures in a flow has first been given by Baudet *et al.* [*Baudet et al.*, 1991] in the canonical configuration of the von Kármán vortex street behind a cylinder at low Reynolds number. Since then, the technique has been ported to turbulent flow at moderate Reynolds number (in a turbulent jet of air [*Poulain et al.*, 2004]) and at high Reynolds number (in a cryogenic turbulent jet of gaseous Helium [*Bezaguet et al.*, 2002; *Pietropinto et al.*, 1999]). Figure 15 shows the schematic of the implementation of acoustical measurement of vorticity in a turbulent jet as done by Poulain *et al.* [*Poulain et al.*, 2004]. In this experiment acoustic transducers are of Sell type consisting of a circular plane piston, with typical diameter of the order of 10 cm (larger and smaller transducers can be used depending on the extent of the flow to be probed), made of a thin mylar sheet (typically

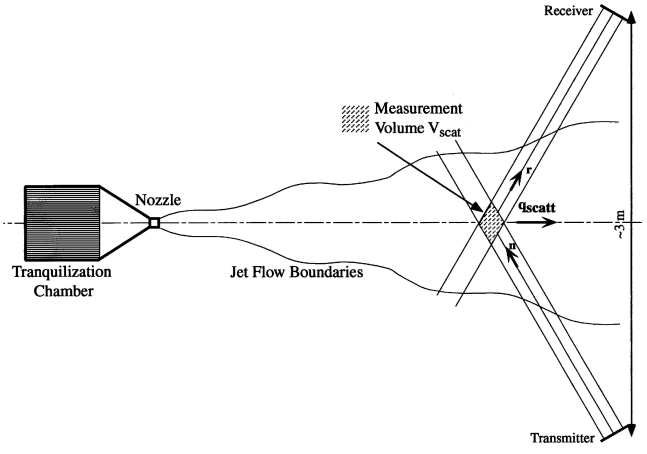

Figure 15. Exemple of implementation of vorticity measurement by acoustic scattering in a turbulent jet (image taken from [*Poulain et al.*, 2004]. Note that the same configuration is can be easily ported to open flows and in city measurements in the atmospheric boundary layer for instance.)

15 μm thickness). One important advantage of such transducers is their large band-width (typically between 1 kHz and 200 kHz in air) which allows to span a wide range of scattering wave-vectors $\vec{q}_{\rm scat}$ with a fixed geometrical arrangement (in particular with a fixed scattering angle). In the present example, the scattering angle was kept fixed at constant value of the order of 60°. The choice of the working scattering angles responds to several criteria : (i) given the angular factor dependence shown in figure 14 angles close to 90° and 180° should be avoided; (ii) at small scattering angles the angular factor increases rapidly, however unless thermal conditions in the experiment are very well controlled small scattering angles should be avoided as forward sound scattering is very sensitive to temperature gradients ; (iii) other practical criteria include for instance geometrical constraints around the experiment, limitation of echoing effects and direct acoustic "blinding" from the emitter to the receiver (in particular via the secondary diffraction side-lobes of the transducers) ; (iv) but beyond these practical considerations, the scattering angle should also be chosen in accordance to the physical properties of the flow to be probed. As already discussed the amplitude of the scattering vector $q_{\rm scat} = 4\pi\nu_0/c\sin(\theta_{\rm scat}/2)$ defines the wave number at which the vorticity spectrum is being probed. It can be selected by changing either the working frequency or the scattering angle. Hence, the scattering angle will be chosen so that wave numbers relevant to the investigated problem can be effectively spanned within the accessible range of operating frequencies of the acoustic transducers. In the present case, an angle of 60° allowed the authors to probe a significant range of the inertial scales of the turbulent jet with a constant scattering angle by simply varying the working frequency ν_0 of the transducers.

As an example of results which can be obtained with this technique, we show in figure 16a a typical power spectrum of the signal recorded by the acoustic receiver (note that the signal has been down-mixed exactly in the same way as explained for the acoustic Lagrangian measurement in the previous section). The maximum of the power spectrum occurs for a non-zero frequency which corresponds to the Doppler shift related to the average velocity of the jet at the location of the measurement volume. The range of detected frequencies around this maximum corresponds to the range of velocity statistically sampled by the vortices in the flow (within the range of spatial scales selected according to the wave-number $q_{\rm scat}$) which scattered the acoustic wave. As a consequence, the shape of the power spectrum directly reflects the statistical properties of the velocity field of the flow. It is a gaussian, centered around a frequency which corresponds to the mean stream velocity of the jet flow at the location of the measurement volume and the width of the gaussian corresponds to the standard deviation of the carrier velocity field. Poulain *et al.* have indeed shown that in their turbulent jet the power spectrum is well fitted by a gaussian :

$$PSD_{\rm scat}(\delta\nu) = \frac{A(\nu_0)}{\sqrt{2\pi}\delta\nu_{rms}} e^{-\frac{(\delta\nu-\delta\nu_{avg})^2}{2\delta\nu_{rms}^2}} \qquad (8)$$

and they have shown that the fitting Doppler shift frequencies $\delta\nu_{avg}$ and $\delta\nu_{rms}$ where in excellent agreement with hot-wire anemometry measurements of the mean and rms velocity of the jet flow.

But more interestingly, they have shown that the quantity $q_{\rm scat}^2 A(\nu_0)$ (where $A(\nu_0)$ is the maximum of the power spectral density) gives a direct estimate of the enstrophy spectrum of the flow at the given wave-number $q_{\rm scat}$, once the transfer function $H(\nu_0)$ between the receiver and the emitter is applied (an important aspect to be considered when using this methods concerns indeed the calibration of the acoustic transducers: while this is not crucial for the Lagrangian measurement previously described, which only relies on the frequency shift information of the scattered wave, a proper calibration of the transfer functions of the receiver and the emitter is required to extract the vorticity information, which is coded in the amplitude of the power spectral density). By varying the working frequency ν_0 (and hence the scattering wave-number $q_{\rm scat}$), it is then possible to reconstruct the entire spectrum of enstrophy what remains one of the most difficult quantities to measure in fluid mechanics experiments. Figure 16b shows the enstrophy spectrum of the jet flow investigated by Poulain *et al.* which they found to be in reasonable agreeement with Kolmogorov phenomenology of turbulence.

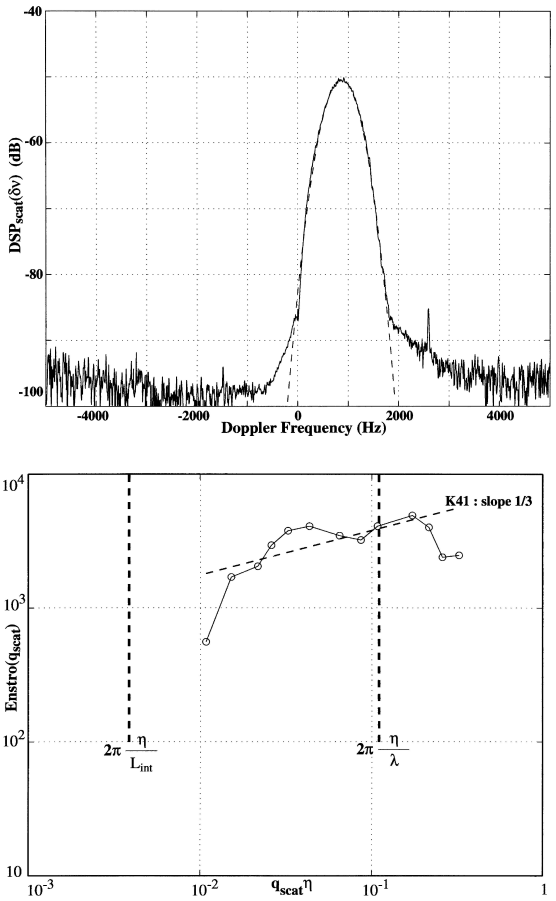

Figure 16. (a) Power spectral density of the signal scattered by the flow. (b) Discrete reconstruction of the spatial spectrum of the flow enstrophy. (Images are taken from [*Poulain et al.*, 2004].)

4. Instrumented particles

When performing Lagrangian measurement in a fluid flow, one is usually limited in track length because of the necessary finite size of the measurement volume. Using Particle Tracking Velocimetry or Doppler Velocimetry one is also limited in the investigation of kinematic quantities (velocity, acceleration, vorticity, ...) although scalar quantities such as salinity or temperature may also be interesting in the cases of geophysical or industrial flows. One may therefore want to use instrumented particles (called smart

particles) with embarked electronics able to measure scalar or kinematic quantities in Lagrangian frame while continuously transmitting the information to the operator for data storage and post-processing.

4.1. Lagrangian temperature measurement

A smart particle has been designed to measure continuously temperature along the particle trajectory using 4 thermistors, placed at the surface of the particle directly in contact with the fluid [*Gasteuil et al.*, 2007; *Shew et al.*, 2007]. It is made of a spherical capsule of diameter $D = 21$ mm containing temperature instrumentation, a Radio Frequency (RF) emitter and a battery. It uses a resistance controlled oscillator LMC555 timer to create a square wave whose frequency depends on the temperature of the several thermistors. This square wave is used directly to modulate the frequency of the radio wave generated by the RF emitter in the range $[22 - 26]$ kHz about the carrying frequency $f_0 = 315$ MHz (see figure 17 and reference [*Shew et al.*, 2007] for more details). The entire mobile circuit is powered with a coin cell battery which conditions the duration of the measurement, about 3 hours. Using an antenna and radio frequency RF receiver and amplifiers, it is possible to acquire directly the demodulated signal oversampling with a high speed DACQ. The square wave signal frequency is then directly measured using standard Labview library, and time varying frequency converted to temperature using frequency-temperature calibration of the thermistors. The time resolution for this distant temperature measurement is about 10 Hz which was suitable for studying turbulent convection in laboratory experiments.

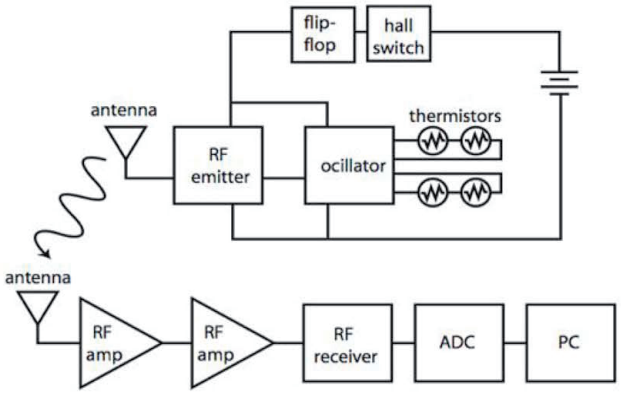

Figure 17. The smart particle measuring temperature uses four thermistors, placed directly in contact with the fluid, connected to a LMC555 timer to generate a square wave with frequency in the range $[22-26]$ kHz depending on the flow temperature [*Gasteuil et al.*, 2007; *Shew et al.*, 2007]. A pair of RF emitter and receiver (MAX7044 and MAX1473 from Maxim Integrated Products) are used for frequency modulation and demodulation at 315 MHz. The emitter antenna is placed inside the capsule with emitting circuit tuned for emission at 315 MHz using a variable capacitor. The signal is received by a fixed antenna, amplified and demodulated before acquisition at 10 MHz with high speed DACQ. The slowly varying frequency of the square wave is then continuously measured using Labview standard library, then stored for further data analysis. Hall switch and flip-flop are used for turning on and off the particle approaching a magnet close to the particle in order to save battery when the experiment is not running.

Measurement in Rayleigh Benard convection The particle was used to investigate natural convection in a square tank with size 30 cm at high Rayleigh numbers $Ra \sim 10^{10}$. Figure 18(up) shows the time evolution of temperature along the particle trajectory with irregular oscillations caused by the motion of the particle crossing cold and hot regions in the vessel. Combining lagrangian temperature measurement and Particle Tracking Velocimetry, it becomes possible to study the correlations between position and temperature as shown in figure 18(down). As all kinematic quantities (velocity or acceleration) can be obtained from PTV data it is then possible to have informations about the turbulent heat flux $q = \langle v'T' \rangle$ (with v' and T' fluctuating velocity and temperature) in the whole experiment volume with insight form the role of plumes in heat transport [*Gasteuil et al.*, 2007; *Shew et al.*, 2007].

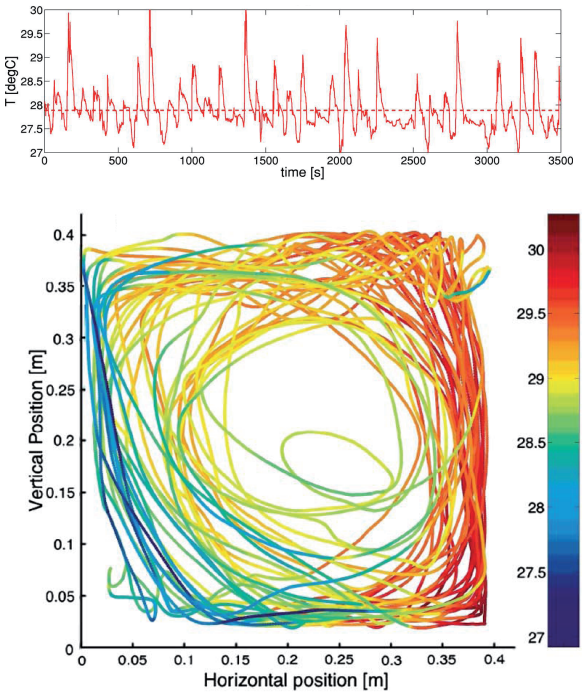

Figure 18. Up : Temporal evolution of temperature along a particle trajectory in turbulent Rayleigh Benard convection with square aspect-ratio. Down : combined PTV-instrumented particle measurement showing the 2d position of the particle $(X(t), Y(t))$ with local temperature $T(t)$ (see colorbar for for values of temperature in Celsius).

4.2. Lagrangian acceleration measurements

More recently the Smart Particle concept was extended to vectorial measurement (i.e. measurement of acceleration) using numerical modulation and demodulation with suitable electronics [*Zimmermann et al.*, 2012]. The apparatus was designed from the work [*Gasteuil*, 2009], and built by smartINST S.A.S., an offspring company from CNRS and ENS de Lyon. It is a spherical particle with diameter 25 mm which embarks an autonomous circuit with 3D-acceleration sensor, a coin cell and a wireless transmission system. It transfers the measured data to a data acquisition center (smartCENTER) which decodes, processes, and stores the signal delivered by the smart particle (figure 19). The smart particle and smartCENTER measure, display and store the three dimensional acceleration vectors acting on the particle as it is advected in the flow.

Figure 19. Left : opened smart particle with embarked electronic circuit built by smartINST S.A.S. Right : processing and display unit (smartCENTER).

Sensor : Thanks to recent development of smart phones, it is now possible to obtain small, low consumption, electronic devices to measure acceleration or magnetic fields. Such an accelerometer is the ADXL 330 (Analog Device) – a three axis accelerometer which returns a voltage proportional to the force acting on a small, movably mounted mass-load suspended by micro-fabricated springs. The three axes of the ADXL 330 are decoupled and form an orthogonal coordinate system attached to the chip package. This arrangement yields a 3D measurement o acceleration, including gravity, with a full scale of +/- 3g. The sensor has to be calibrated to compute the physical accelerations from the voltages of the accelerometer.

Description of the embarked acceleration measurement : The smart particle uses numerical modulation which allows for high sample rates and transmission of several measurements at the same time. For measurement at 316 Hz (maximum frequency sampling presently accessible), signals are first-order low-pass filtered at $f_c = 160$ Hz to avoid aliasing problem, and then digitized with 12 bits DACQ with corresponding sampling rate. The three components are then multiplexed for serial transmission with only one carrying frequency before the output is reshaped into small packets and sent via radio frequency.
The ADXL 330 is soldered to the printed circuit board such that it is situated close to the geometrical center of the particle. The particle itself is spherical with a diameter of 25 mm, large enough either for including a battery with long life time or for matching in density the particle and fluids within a range of $[0.8 - 1.4]$ g/cm^3. The particle is then suited for most experiments in water and water-based solutions.
The signals from the particle are received by an antenna connected to a radio reception, processing and display unit (figure 19). It demodulates and decodes in real-time the received raw signal into a time-series of raw voltages of the ADXL 330. The physical acceleration sensed by the smart particle $\vec{a}_{\rm SP}$ are then computed according to the formula :

$$\vec{a}_{\rm SP} = \begin{pmatrix} a_1 \\ a_2 \\ a_3 \end{pmatrix} = \begin{pmatrix} (A_1 - O_1)/S_1 \\ (A_2 - O_2)/S_2 \\ (A_3 - O_3)/S_3 \end{pmatrix}, \qquad (9)$$

where A_i, O_i and S_i are the measured raw signal, the offset and the sensitivity of each axis, respectively. The resulting time-series are saved for further processing.

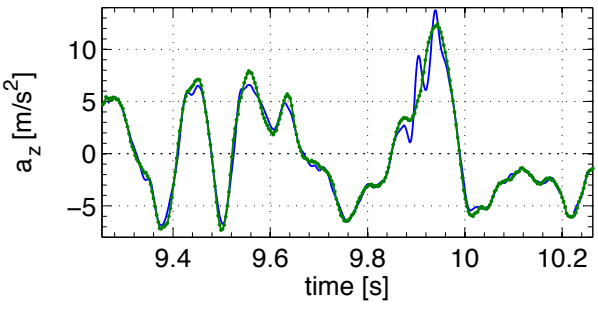

Figure 20. A sample trajectory of the instrumented particle seen by the camera (−) or smartPART (•), in a turbulent von Kármán flow with counter rotating discs at 180 rpm. The absolute orientation of the particle was used to re-express the smartPART measurement and camera measurement in the lab frame. Gravity was subtracted.

Calibration : In order to perform precise acceleration measurements, the offset and sensitivity of the accelerometer have to be calibrated to convert the measured voltages into a physical acceleration. Due to sensitive temperature characteristics of gain and offset, this has to be done before at the mean temperature of the experiment. As it difficult to change gravity to perform calibration, the common technique is to use the property of the accelerometer to measure the three components of gravity $\vec{g}$ forming a orthogonal coordinate system according to Eq. (19). At rest one observes always gravity projected on the sensor at an arbitrary orientation. The square of the observed accelerations always define belong to a translated ellipsoid $\vec{a}_{\rm SP} \cdot \vec{a}_{\rm SP} = \sum_i (A_i - O_i)^2/S_i^2 = g^2$. A sufficient number of measurements with different orientations define a set of equations which is solved using a linear least squares technique to obtain offsets and sensitivities for the different axes [*Zimmermann et al.*, 2012].

Acceleration data : Lagrangian acceleration measurements were performed in a fully turbulent von Kármán flow in order to test further the smart particle [*Zimmermann et al.*, 2012]. Simultaneous PTV was performed using Phantom V.12 fast cameras (with sampling frequency 1 kHz) in order to have a precise comparison between acceleration data either measured by the smartPART or acceleration obtained from its position. The absolute orientation of the particle was measured following the procedure [*Zimmermann et al.*, 2011a, b] in order to project the two measurements in the laboratory frame. Typical data from the two systems is displayed in figure 20. The agreement between the raw acceleration measured by the smart particle was observed to be in very good agreement with PTV data except for rapid oscillations which may be filtered out by the smartPART ADC.
Although a 316 Hz sampling frequency maybe enough for most geophysical flows, increasing the sampling frequency of the device is still an issue for very turbulent flows.

Salinity measurement : The smart particle technology allows for transmitting additional information (with decreased sampling frequency) originating from an other measurement. It is thus possible to use the particle for simultaneous measurement of temperature (through a resistance measurement). Further development for conductivity measurement using small electrodes are under development, such salinity measurements may be promising for geophysical applications, especially for studying mixing in stratified flows.

5. Conclusion

We have presented among the latest developments in characterization of flows in laboratory experiments, mainly in the context of a Lagrangian description. The different presented techniques have each their advantages and drawbacks. High resolution optical tracking has become one of the most accurate techniques in experimental fluid mechanics. It allows to track simultaneously hundreds of particles in 3D allowing to address crucial questions, related for instance to mixing and transport properties of flows. Its main drawback is its cost several high speed cameras are generally required. Acoustic tracking and ELDV, both based on Doppler velocimetry are more affordable techniques, though they are limited to the tracking of essentially one particle at a time and are therefore not adapted to multi-particle studies. Their main advantage relies however on the fact that they give a direct measurement of particle velocity (and not particle position as in optical tracking) hence limiting the increase of noise induced by the differentiation of position to access velocity. Similarly, measuring acceleration of the particles requires only one differentiation step while second derivatives must be estimated from optical tracking. These techniques are therefore very accurate to investigate the Lagrangian dynamics of individual particles. Instrumented particles have ported further the capacity of investigation of Lagrangian properties of flows by giving access not only to kinematic properties (as velocity or acceleration) but also to a Lagrangian description of almost any physical quantity for which a relevant sensor can be embedded in the particle. The main drawback for the moment concerns the size of the particle which does not allow to probe scales smaller than about 1 cm. Finally the acoustical vorticity measurement is unique of its kind as it gives a simple and accurate way to characterize the enstrophy spectrum of a flow, with intrinsic spectral resolution at a selected scale (including the smallest scales of the flow, which are hardly accessible with classical techniques as PIV).

Note that we have not presented here all the possible extensions and add-ons of these methods as for instance the use of digital holography [*Salazar et al.*, 2008; *Chareyron*, 2009] which allows to track particles in 3D with one single camera, or the tracking of particles rotational dynamics [*Zimmermann et al.*, 2011b; **?**; *Klein et al.*, 2012] which allows to simultaneously investigate the translation and rotation of finite objects transported in a flow.

Let us finish by mentioning that experimental techniques in fluid mechanics are constantly improved, as new ideas combined to technological advances increase the resolution and the range of existing methods : cameras are for instance ever faster and sensors better resolved ; miniaturization and reduction of power consumption of electronic components will progressivelly allow to reduce the size of instrumented particles ; an important breakthrough in high resolution optical tracking is expected in the coming years thanks to FPGA (Field Programmable Gate Array) technology which allows to process images on-board and hence to increase the effective data rate (for instance, particle detection could be done on-board and only the particle positions would be recorded, what can be downloaded from the camera much faster than a complete series mega-pixels images). In this rapidly evolving context an efficient interaction between fluid mechanics experimentalists and other communities, and in particular the geophysical one, is crucial in order to develop appropriate instrumentation to address relevant questions in laboratory models.

References

Ayyalasomayajula, S., A. Gylfason, L. R. Collins, E. Bodenschatz, and Z. Warhaft, Lagrangian measurements of inertial particle accelerations in grid generated wind tunnel turbulence, *Physical Review Letters*, *97*, 144,507, 2006.

Batchelor, G. K., Wave scattering due to turbulence, in *Symposium on Naval-Hydrodynamics*, edited by F. S. Sherman, pp. 403–429, National Academy of Sciences, Washington, 1957.

Baudet, C., S. Ciliberto, and J.-F. Pinton, Spectral analysis of the von Karman flow using ultrasound scattering, *Physical Review Letters*, *67*, 193–195, 1991.

Bezaguet, A., et al., A cryogenic high Reynolds turbulence experiment at CERN, *Adv. Cryo. Eng.*, *47*, 136–144, 2002.

Bourgoin, M., N. T. Ouellette, H. T. Xu, J. Berg, and E. Bodenschatz, The role of pair dispersion in turbulent flow, *Science*, *311*(5762), 835–838, doi:DOI 10.1126/science.1121726, 2006.

Bourgoin, M., N. M. Qureshi, C. Baudet, A. Cartellier, and C. Gagne, Turbulent transport of finite sized material particles, *Journal of Physics: Conference Series*, *318*(1), 012,005, doi:10.1088/1742-6596/318/1/012005, 2011.

Brown, R. D., Z. Warhaft, and G. A. Voth, Acceleration Statistics of Neutrally Buoyant Spherical Particles in Intense Turbulence, *PHYSICAL REVIEW LETTERS*, *103*(19), doi:10.1103/PhysRevLett.103.194501, 2009.

Chareyron, D., Développement de méthodes instrumentales en vue de l'étude Lagrangienne de l'évaporation dans une turbulence homogène isotrope, Ph.D. thesis, Ecole Centrale de Lyon, 2009.

Chu, B. T., Non-Linear interactions in a viscous heat-conducting compressible gas, *Journal of Fluid Mechanics*, *3*, 494–514, 1958.

Colonius, T., S. K. Lele, and P. Moin, The scattering of sound waves by a vortex: numerical and analytical solutions, *Journal of Fluid Mechanics*, *260*(10), 271–298, 1994.

Del Castello, L., and H. J. H. Clercx, Lagrangian acceleration of passive tracers in statistically steady rotating turbulence, *Physical Review Letters*, *107*, 214,502, 2011.

Flandrin, P., *Time-Frequency/Time-Scale Analysis*, Academic Press, New York, 1998.

Gasteuil, Y., Instrumentation Lagrangienne en Turbulence: Mise en oeuvre et Analyse, Ph.D. thesis, ENS Lyon, 2009.

Gasteuil, Y., W. L. Shew, M. Gibert, F. Chillà, B. Castaing, and J.-F. Pinton, Lagrangian temperature, velocity, and local heat flux measurement in Rayleigh-B{é}nard convection, *Phys. ˜Rev. ˜Lett.*, *99*(23), 234,302, 2007.

Klein, S., M. Gibert, and B. Antoine, Simultaneous 3D measurement of the translation and rotation of finite size particles and the flow field in a fully developed turbulent water flow ., *ArXiv*, p. arXiv:1205.2181v1, 2012.

Kodera, K., C. de Villedary, and R. Gendrin, A new method for the numerical analysis of nonstationary signals, *Physics of the Earth and Planetary Interiors*, *12*, 142–150, 1976.

Kraichnan, R. H., The scattering of sound in a turbulent medium, *J. Acoust. Soc. Am.*, *25*, 1096–1104, 1953.

LaPorta, A., G. A. Voth, A. M. Crawford, J. Alexander, and E. Bodenschatz, Fluid particle accelerations in fuly developped turbulence, *Nature*, *409*, 1017, 2001.

Llewellyn Smith, S. G., and R. Fort, Three dimensional acoustic scattering by vortical flows, *Physics of Fluids*, *13*(10), 2876–2889, 2001.

Lund, F., and C. Rojas, Ultrasound as a Probe of Turbulence, *Physica D*, *37*, 508–514, 1989.

Mordant, N., Mesure lagrangienne en turbulence : mise en œuvre et analyse, Ph.D. thesis, Ecole Normale Supérieure de Lyon, 2001.

Mordant, N., P. Metz, O. Michel, and J.-F. Pinton, Measurement of Lagrangian Velocity in Fully Developed Turbulence, *Physical Review Letters*, *87*(21), 214,501, 2001.

Mordant, N., J.-F. Pinton, and O. Michel, Time-resolved tracking of a sound scatterer in a complex flow: Nonstationary signal analysis and applications, *Journal of the Acoustical Society of America*, *112*(1), 108–118, 2002.

Mordant, N., P. Metz, J. F. Pinton, and O. Michel, Acoustical technique for Lagrangian velocity measurement, *Review of Scientific Instruments*, *76*(2), 25,105, 2005.

Obukhov, A. M., Effect of weak inhomogeneities in the atmosphere on sound and light propagation, *Izv. Akad. Nauk. Seriya Geofiz.*, *2*, 155–165, 1953.

Ott, S., and J. Mann, An experimental investigation of the relative diffusion of particle pairs in three-dimensional turbulent flow, *Journal of Fluid Mechanics*, *422*, 207–223, 2000.

Ouellette, N. T., H. Xu, and E. Bodenschatz, A quantitaive study of three-dimensional Lagrangian particle tracking algorithms, *Experiments in Fluids*, *39*(4), 722–729, 2005.

Pietropinto, S., et al., Superconducting instrumentation for high Reynolds turbulence experiments with low temperature gaseous helium, *Physica C*, *386*, 512–516, 1999.

Poulain, C., N. Mazellier, P. Gervais, Y. Gagne, and C. Baudet, Spectral vorticity and Lagrangian velocity measurements in turbulent jets, *Flow, Turbulence and Combustion*, *72*, 245–271, 2004.

Qureshi, N., Experimental Investigation of Finite Sized Inertial Particles Dynamics in Wind Tunnel Grid Generated Turbulence, Ph.D. thesis, Université Joseph Fourier - Grenoble I, 2009.

Qureshi, N. M., M. Bourgoin, C. Baudet, A. Cartellier, and Y. Gagne, Turbulent transport of material particles: An experimental study of finite size effects, *Physical Review Letters*, *99*(18), doi:DOI 10.1103/PhysRevLett.99.184502, 2007.

Qureshi, N. M., U. Arrieta, C. Baudet, A. Cartellier, Y. Gagne, and M. Bourgoin, Acceleration statistics of inertial particles in turbulent flow, *European Physical Journal B*, *66*(4), 531–536, doi:DOI 10.1140/epjb/e2008-00460-x, 2008.

Salazar, J. P. L. C., J. de Jong, L. Cao, S. H. Woodward, H. Meng, and L. R. Collins, Experimental and numerical investigation of inertial particle clustering in isotropic turbulence, *Journal of Fluid Mechanics*, *600*, 245–256, 2008.

Shew, W. L., Y. Gasteuil, M. Gibert, P. Metz, and J.-F. Pinton, Instrumented tracer for Lagrangian measurements in Rayleigh-B{é}nard convection, *Rev. ˜Sci. ˜Instru.*, *78*(6), 65,105, 2007.

Tennekes, H., and J. L. Lumley, *A first course in turbulence*, MIT press, 1992.

Tsai, R., A versatile camera calibration technique for high accuracy 3d machine vision metrology using off-the-shelf tv cameras and lenses, *IEEE T. Robot. Autom.*, *RA-3*, 323, 1987.

Virant, M., and T. Dracos, {3D} {PTV} and its application on lagrangian motion, *Measurement science and technology*, *8*, 1539–1552, 1997.

Volk, R., N. Mordant, G. Verhille, and J.-F. Pinton, Laser Doppler measurement of inertial particle and bubble accelerations in turbulence, *European Physics Letters*, *81*, 34,002, 2008.

Volk, R., E. Calzavarini, E. Leveque, and J. Pinton, Dynamics of inertial particles in a turbulent von karman flow, *to appear in J Fluid Mech*, 2010.

Voth, G. A., A. LaPorta, A. M. Crawford, J. Alexander, and E. Bodenschatz, Measurement of particle accelerations in fully developed turbulence, *Journal of Fluid Mechanics*, *469*, 121–160, 2002.

Xu, H., and E. Bodenschatz, Motion of inertial particles with size larger than Kolmogorov scale in turbulent flows, *Physica D: Nonlinear Phenomena*, *237*(14-17), 2095–2100, doi:10.1016/j.physd.2008.04.022, 2008.

Zimmermann, R., Y. Gasteuil, M. Bourgoin, R. Volk, A. Pumir, and J.-F. Pinton, Tracking the dynamics of translation and absolute orientation of a sphere in a turbulent flow, *Review of Scientific Instruments*, *82*, 033,906, 2011a.

Zimmermann, R., Y. Gasteuil, M. Bourgoin, R. Volk, A. Pumir, and J.-F. Pinton, Rotational Intermittency and Turbulence Induced Lift Experienced by Large Particles in a Turbulent Flow, *Physical Review Letters*, *106*(15), 154,501, doi:DOI 10.1103/PhysRevLett.106.154501, 2011b.

Zimmermann, R., L. Fiabane, Y. Gasteuil, R. Volk, and J.-F. Pinton, Measuring lagrangian accelerations using an instrumented particle, *Arxiv*, 2012.

M. Bourgoin, Laboratoire des Écoulements Géophysiques et Industriels, CNRS/UJF/GINP - Université de Grenoble, BP53 - 38041 Grenoble Cedex 9, France. (mickael.bourgoin@legi.grenoble-inp.fr)

J.-F. Pinton, Laboratoire de Physique de l'École Normale Supérieure de Lyon, 46 Allée d'Italie, 69007 Lyon, France.

R. Volk, Laboratoire de Physique de l'École Normale Supérieure de Lyon, 46 Allée d'Italie, 69007 Lyon, France.